12 Surface Physics

T. Greber, M. Hengsberger, J. H. Dil, H. Yanagisawa, H. Ma, C. Galli-Marxer, C. Hengsberger, M. Morscher, T. Brugger, F. Meier, D. Leuenberger, S. Roth, J. Schmidlin, M. Thomann, D. Böni, P. Donà, M. Hausherr, M. Klöckner, J. Osterwalder

In the surface physics group model systems of well defined surfaces and interfaces are systematically studied in order to address fundamental issues that are potentially relevant for nanoscience and nanotechnology. Our laboratory is well equipped for the preparation and characterization of clean surfaces, ultrathin metal films, molecular monolayers and covalently bonded single layers like hexagonal boron nitride or graphene, all under ultrahigh vacuum (UHV) conditions. Techniques available to us include x-ray photoelectron spectroscopy (XPS) and diffraction (XPD), angle-resolved photoemission spectroscopy (ARPES), two-photon photoemission (2PPE) using femtosecond laser pulses, low-energy electron diffraction (LEED) and variable-temperature scanning tunneling microscopy (STM). At the nearby Swiss Light Source (SLS) we operate two more photoemission spectrometers, one for spin- and angle-resolved photoemission spectroscopy (SARPES) and one for photoelectron diffraction and holography. A growing network of national and international collaborations expands this set of techniques and provides us also with the necessary theoretical support.

The research carried out during the report period can be grouped into four topics:

- **Monolayer films of hexagonal boron nitride and graphene on metal surfaces**
  The boron nitride nanomesh is a one atom thick layer of hexagonal boron nitride (h-BN) on Rh(111) surfaces, which we discovered a few years ago (1). It exhibits a very regular hexagonal corrugation pattern with 2 nm wide "holes", i.e. regions where the layer is more strongly bonded to the metal surface, and a periodicity of 3.2 nm, giving the surface a mesh-like appearance in STM images. We have continued the studies of Co cluster formation on the nanomesh by adsorbing Co carbonyls. Preliminary results indicate that these molecules strip off their carbonyl groups completely and, when deposited at low temperatures (50 K), tend to form rather monodisperse ultrasmall clusters inside the holes. In the context of a new collaborative SNF SINERGIA project (since 1 October 2008), where the nanomesh template functionality in solutions is explored, our main activity is the study of the adsorption of water molecules on the nanomesh. Low-temperature STM images show the formation of monodisperse two-dimensional ice crystals. In the course or two Master projects (J. Schmidlin and Mario Thomann), our room temperature STM was equipped with a detector for photons excited locally by the tunneling current from the tip. Recently a clear contrast with the nanomesh periodicity could be observed on a h-BN covered Rh(111) surface. Finally, we have extended our activities in the field of sp^2 bonded monolayer networks to the closely related systems of graphene on transition metal surfaces. A direct comparison of the properties of graphene and boron nitride monolayers on the Ru(0001) surface are presented in Sec. 12.1.

- **Ultrafast processes at surfaces**
  Using femtosecond laser pulses from an amplified laser system, time-resolved photoemission can be used to observe fast electron dynamics at surfaces. Two major projects have been pursued and successfully finished last year. Image poten-

tial states, which exist in front of metal surfaces, may be spin-split due to the exchange-split bandstructure of the metal. Such a state has been identified in front of the h-BN/Ni(111)-surface investigated here. It can be exited resonantly using the second harmonic from a Ti:Sa laser system (2). The energy position of the image potential state is sensitive to the magnetic phase and can be used as an ultrafast thermometer for the phenomenological spin temperature in the surface region of the metal. By means of an intense infrared pump pulse, energy is pumped into the system, leading to the reduction of the magnetic moment within a few hundred femtoseconds (3). As a consequence of the enhanced electron temperature, the transient position of the image potential state shifts towards higher energies within about 200 fs after the pump pulse. This shift can be related to spin disorder resulting in an effective spin temperature close to the Curie temperature of bulk nickel.

The second project concerned time- and angle-resolved photoelectron spectroscopy from a self-assembled monolayer of tetramantane molecules absorbed onto Ag(111) and Au(111) surfaces. Tetramantane is the first member of the class of higher diamondoids, which are small nanometer-sized molecules of carbon atoms in a diamond structure (4). These monolayer systems were previously shown, using synchrotron radiation, to have a negative electron affinity (5). They represent thus very efficient electron emitters. Using a widely tunable parametric amplifier as light source, a threshold behavior was found for the excitation yield. This threshold could be related to the substrate bandstructure. Moreover, the experiments allowed the angular emission cone to be measured and the value of the negative electron affinity to be estimated. From these and further time-resolved measurements we conclude that the initial excitation takes place in the substrate. Furthermore, the retention time of the electrons in the diamondoid orbital before emission could be estimated to be below 2 fs, indicating a very efficient charge transfer from the substrate to this orbital and subsequent emission into vacuum.

In parallel to these efforts, photon-assisted field emission from sharp W-tips was studied by using infrared pulses from the laser oscillator. In order to characterize the tips and the electron-emission intensity patterns, a position-sensitive, microchannelplate amplified electron detector was used. For this purpose new read-out electronics and data acquisition routines were implemented within a Bachelor project (P. Donà). The emission patterns show a very distinct asymmetry, which is related to the propagation direction of the light field. These patterns are currently being simulated by using finite-element methods.

- **Spin-resolved photoemission and momentum mapping**

  Our spin-resolved photoemission chamber at the SLS (COPHEE, the complete photoemission experiment) has been upgraded with new high voltage electronics for the Mott detectors, which has resulted in a further increase of the detection efficiency and in the operation stability. The combination of the unique capabilities of COPHEE with the two step analysis routine we developed last year (6) has resulted in a variety of new and unexpected results. We have, for example, been able to measure a spin splitting of Pb quantum well states which is not accessible with spin integrated ARPES (see Sec. 12.2). Further have we been able to provide the first direct experimental observation of the quantum spin Hall phase on the surface of a BiSb alloy (7). In order to determine the influence of reduced dimensionality on the spin structure of surfaces, we have performed SARPES measurements on the

Bi(114) vicinal surface. The Fermi surface of this system primarily consists of a pair of one-dimensional spin split bands (8). Because all electrons at the surface with positive momentum have spin up and all electrons with negative momentum spin down, Bi(114) can be considered as the parent compound of a one-dimensional quantum spin Hall system.

- **Further instrumental developments**
  For molecules adsorbed on ferromagnetic surfaces the spin-dependent coupling of molecular orbitals to states of the underlying substrate can be studied. In order to exploit the versatile preparation and characterization environment of our photoelectron spectrometer chamber, we have engaged in a development project for a simplified type of spin detector that is compatible with the existing hemispherical electron analyzer. In this new type of Mott detector, backscattered high-energy electrons are measured within scintillators. The light pulses are extracted by glass rods out of the UHV. A first prototype has been built and is currently undergoing tests.

  For more efficient studies of ultrafast phenomena on surfaces by means of time-resolved photoemission, a new electron display analyzer has been implemented, which allows the whole angular distribution of photoelectrons at a given energy to be recorded in one shot (9). The commissioning included the setup of a new vacuum system and building a new sample manipulator. Within a new Bachelor project (M. Hausherr) the visible light pulses of the second harmonic of the Ti:Sa laser are again frequency-doubled to about 6 eV in a new β-barium-borate crystal and coupled into the vacuum system by using a SrF_2-viewport, which is transparent for uv-radiation.

In the following, two highlights of last year's research are presented in more detail.

12.1 Comparison of single-layer graphene and hexagonal boron nitride on Ru(0001)

in collaboration with: S.Günther and J. Wintterlin, Department Chemie, Ludwig-Maximilian Universität, D-81377 München, Germany; B. Wang and M.-L. Bocquet, Laboratoire de Chimie, Université de Lyon, Ecole Normale Suprieure de Lyon, CNRS, F-69007 Lyon, France; D. Martoccia and P. R. Willmott, Swiss Light Source, Paul Scherrer Institut, CH-5232 Villigen, Switzerland.

Graphene and hexagonal boron nitride (*h*-BN) are isoelectronic sp^2 hybrid-bonded networks that can be grown on transition metals (10). For the case of h-BN/Rh(111) the formation of a nanomesh with new functionalities has been reported (1; 11; 12). Grown on Ru(0001) h-BN (13) and graphene (g) (14) also form large supercells, with lattice constants of about 3 nm, that are caused by the lattice mismatch between the sp^2 network and the substrate. For g/Ru(0001) surface X-ray diffraction showed a surprisingly large (23x23) unit cell (referenced to the primitive Ru(0001) unit cell) containing four 3 nm subcells (15). The strong site dependence of the interaction to the substrate leads to a corrugation or rippling of the overlayers with a height difference between strongly bonded and weakly bonded regions of the sp^2 networks, which is in the order of 0.1 nm. Bonding occurs wherever nitrogen or carbon atoms sit on top of metal atoms (16; 17). For the graphene layer this condition can be met by either one of the two carbon atoms in the unit cell, while for h-BN there is only one nitrogen atom in the unit cell. The overall area of strongly bonded regions it therefore larger in the graphene case. This has the consequence that the h-BN nanomesh has isolated strongly bonded patches (holes) and graphene has connected, strongly bonded valleys and weakly bonded mounds with a diameter of about 2 nm (18). One layer is in fact

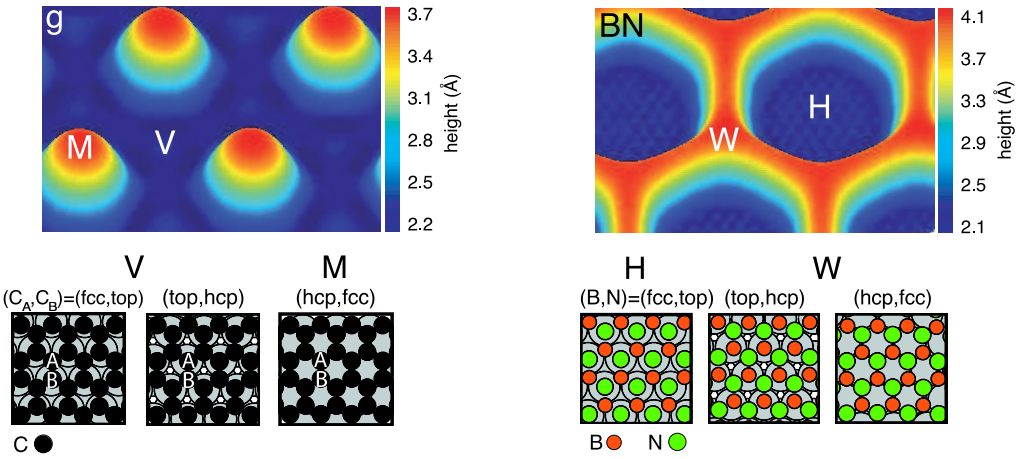

Figure 12.1: Views of the height modulated graphene (g) and h-BN on Ru(0001). M and V denote mounds (high) and valleys (low) of the graphene, H and W holes (low) and wires (high) of the h-BN. The six ball model panels illustrate the three different bonding regions (fcc, top), (top, hcp), and (hcp, fcc).

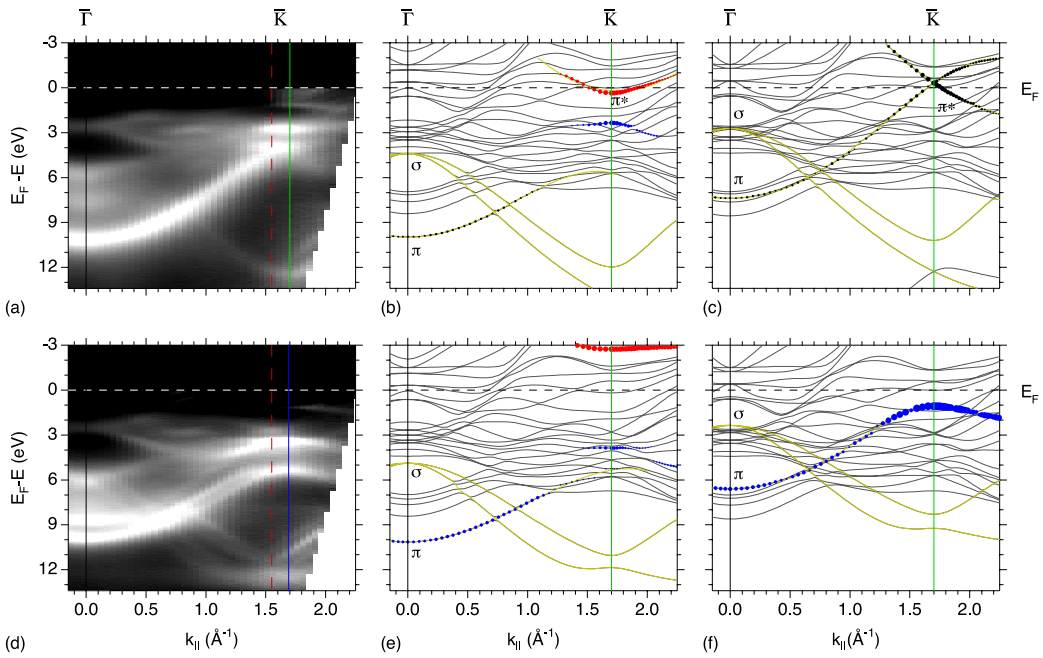

Figure 12.2: Band structures of graphene and h-BN nanomesh on Ru(0001) along $\overline{\Gamma K}$: (a) He II$_\alpha$ photoemission data of g/Ru(0001). (b) and (c) Density Functional Theory (DFT) results of g/Ru(0001) for the low ((C$_A$, C$_B$) (top, hcp)) and high ((C$_A$, C$_B$) (hcp, fcc)) regions, respectively (see Fig. 12.1). (d) He II$_\alpha$ photoemission of h-BN/Ru(0001). (e) and (f) DFT results of h-BN/Ru(0001) for the low ((B, N) (fcc, top)) and high ((B, N) (hcp, fcc)) regions. The vertical lines at and near $\overline{K}$ in (a) and (d) indicate the boundaries of the 1×1 surface Brillouin zones for Ru (red dashed), h-BN (blue solid) and graphene (green solid). The sizes of the dots in the theoretical curves represent the p_z weight of specific adsorbate atoms in the bands, where blue describes atop atoms (C$_A$ in (b) and N in (e)) and red hollow site atoms (C$_B$ in (b) and B in (e)). Black dots in (c) depict the weight averaged over the two carbon atoms in the graphene unit cell. Thick yellow curves are guides for the eyes. From Ref. [18].

reminiscent of the casting mould of the other (see Fig. 12.1). Obviously this may cause similarities and differences in the electronic structure and functionality of the two systems.

The electronic structures along $\overline{\Gamma K}$ in the 1x1 surface Brillouin zones of h-BN/Ru(0001) and g/Ru(0001) show a large π-band gap at the $\overline{K}$ point. For graphene the carbon-substrate interaction causes this gap. It reflects the substrate induced symmetry breaking between the two carbon sublattices C_A and C_B of graphene. A charge transfer of 0.05 electrons per carbon atom to the graphene layer moves this gap fully into the occupied states (Fig. 12.2 a)), with electron pockets forming around the $\overline{K}$ points (18). For h-BN the sublattice symmetry breaking is intrinsic since the nitrogen and the boron network are not even identical in the free standing case - hence the large band gap. Most of these observations (Fig. 12.2 (a, d)) are reproduced by density functional theory (DFT, Fig. 12.2). The gaps and, for the graphene case, the charge transfer are nicely reproduced in calculations for the strongly bonded (low) regions (Fig. 12.2 (b, e)). In the h-BN case, the splitting of the σ and π bands resulting from the contribution of the weakly bonded (high) regions is also reproduced (Fig. 12.2 (f)), while the predicted closing of the gap on the mounds of graphene (Fig. 12.2 (c)) is not seen in our data.

12.2 Rashba-type spin-orbit splitting of quantum well states in ultrathin Pb films

in collaboration with: Luc Patthey, Swiss Light Source, PSI, Villigen, Switzerland and Gustav Bihlmayer, Institut für Festkörperforschung, Forschungszentrum Jülich.

When the thickness of a metal layer is smaller than the electron coherence length, quantum well states (QWS) may form in the layer. Within a simple model these are well described by standing electron waves between the metal-substrate and metal-vacuum interface. We have performed spin and angle resolved photoemission spectroscopy (SARPES) measurements on QWS in thin Pb films. It will be shown that the atomic and electronic structure of the metal-substrate interface provides the essential ingredient for the occurrence of Rashba type spin-orbit splitting of these quantum well states. This is a relativistic effect caused by the effective potential gradient that results from the breaking of the space inversion symmetry at surfaces or interfaces (19). In the reference frame of the electron this is equivalent to an in-plane magnetic field, and in a first approximation bands with opposite spin will be shifted in opposite momentum directions. The size of this band splitting depends on the atomic spin-orbit coupling strength and on the magnitude of the potential gradient, where a larger potential gradient results in a larger splitting.

The metal-vacuum interface and the metal-substrate interface are typically not identical for a thin metal layer, and consequently the space inversion symmetry is broken. Similarly to the situation for metal surface states this should result in the spin splitting of the quantum well states. However, up to now no splitting that can be explained by this mechanism has been observed. It has been shown previously that QWS may show a spin splitting due to hybridization with interface (20) or surface states (21), which either decays with layer thickness or is sensitive to contamination. Here we report the first observation of an intrinsic Rashba type spin-orbit splitting in metallic QWS by SARPES (22). An example of these results is shown in Fig. 12.3. The measured splitting of the Kramers pairs of approximately 15 meV is larger than what is observed in the classical Rashba systems, the two-dimensional electron gases in semiconductor heterostructures (23), but too small to be directly accessible by high resolution ARPES. The additional tag of spin polarization is needed to separate the

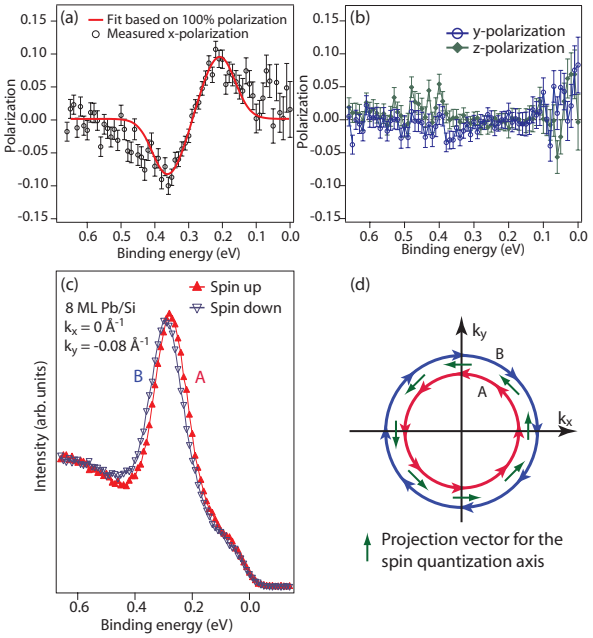

Figure 12.3: Spin and angle resolved photoemission data for an 8 ML thick Pb layer on Si(111)$\sqrt{3}\times\sqrt{3}$ ($R30°$). (a) Measured and modeled spin polarization in the x-direction of the sample. (b) Measured spin polarization along the y and z direction of the sample. (c) Spin resolved spectra obtained from the spin polarization in the x-direction. The splitting between the two peaks is 14 meV. (d) Schematic representation of a constant energy surface where the arrows of band A and B refer to the direction of the spin polarization axis (from Ref. [22]).

two split peaks. Furthermore we find a reversal of the spin orientation with respect to the Au(111) L-gap surface state (24) and no strong dependence on the Pb layer thickness.

The magnitude of the splitting, the spin polarization direction and the absence of a dependence on the layer thickness are explained by the net result of competing effects at both interfaces. This interpretation is corroborated by state-of-the-art density functional theory calculations where the substrate is included (22). This means that the spin-orbit interaction takes place throughout the whole layer, but the necessary asymmetry is induced by the two interfaces of the film. This opens up the possibility to manipulate the Rashba effect by interface engineering. This tunability in combination with the technologically interesting size of the band splitting and the fact that the system is formed on a semiconductor substrate, can provide a next step to the realisation of a spin field effect transistor as proposed by Datta and Das (25) and may benefit other fields of spintronics.

[1] M. Corso et al., Science **303**, 217 (2004).
[2] M. Muntwiler et al., Phys. Rev. B **75**, 075407 (2007).
[3] B. Koopmans et al., J. Magn. Magn. Mat. **286**, 271 (2005).
[4] J.E. Dahl, S.G. Liu, and R.M.K. Carlson, Science **299**, 96 (2003).
[5] W.L. Yang et al., Science **316**, 1460 (2007).
[6] F. Meier et al., Phys. Rev. B **77**, 165431 (2008).
[7] D. Hsieh et al., Science **323**, 919 (2009).
[8] J. W. Wells et al., Phys. Rev. Lett. **102**, 096802 (2009).
[9] T. Dütemeyer et al., Rev. Sci. Instr. **72**, 2638 (2001).
[10] C. Oshima and A. Nagashima, J. Phys.: Condens. Matter **9**, 1 (1997).
[11] S. Berner et al., Angew. Chem. Int. Ed. **46** 5115 (2007).
[12] H. J. Dil et al., Science **319** 1826 (2008).
[13] A. Goriachko et al., Langmuir **23**, 2928 (2007).
[14] S. Marchini, S. Günther and J. Wintterlin, Phys. Rev. B **76**, 075429 (2007).
[15] D. Martoccia et al., Phys. Rev. Lett. **101**, 126102 (2008).
[16] R. Laskowski, P. Blaha, T. Gallauner, and K. Schwarz, Phys. Rev. Lett. **98**, 106802 (2007).
[17] B Wang et al., Phys. Chem. Chem. Phys., **24**,3530 (2008).
[18] T. Brugger et al., Physical Review B, **79**, 045407 (2009).
[19] Y.A. Bychkov and E.I. Rashba, JETP Lett. **39**, 78 (1984).
[20] C. Koitzsch et al., Phys. Rev. Lett. **95**, 126401 (2005).
[21] K. He et al., Phys. Rev. Lett. **101**, 107604 (2008).
[22] J. H. Dil et al., Phys. Rev. Lett. **101**, 266802 (2008).
[23] J. Nitta et al., Phys. Rev. Lett. **78**, 1335 (1997).
[24] M. Hoesch et al., Phys. Rev. B **69**, 241401 (2004).
[25] S. Datta and B. Das, Appl. Phys. Lett. **56**, 665 (1990).